JACS
JOURNAL OF THE AMERICAN CHEMICAL SOCIETY
Article
pubs.acs.org/JACS

Thermophoretic Manipulation of Molecules inside Living Cells

Maren R. Reichl and Dieter Braun*

Systems Biophysics, Physics Department, NanoSystems Initiative Munich and Center for Nanoscience, Ludwig-Maximilians-Universität München, Amalienstrasse 54, 80799 München, Germany

Supporting Information

ABSTRACT: The complexity of biology requires that measurements of biomolecular interactions be performed inside living cells. While electrophoresis inside cells is prohibited by the cell membrane, the movement of molecules along a temperature gradient appears feasible. This thermophoresis could be used to quantify binding affinities *in vitro* at picomolar levels and perform pharmaceutical fragment screens. Here we changed the measurement paradigm to enable measurements inside living cells. The temperature gradient is now applied along the optical axis and measures thermophoretic properties for each pixel of the camera image. We verify the approach for polystyrene beads and DNA of various lengths using finite element modeling. Thermophoresis inside living cells is able to record thermophoretic mobilities and intracellular diffusion coefficients across the whole cytoplasm. Interestingly, we find a 30-fold reduced diffusion coefficient inside the cell, indicating that molecular movement across the cell cytoplasm is slowed down due to molecular crowding.

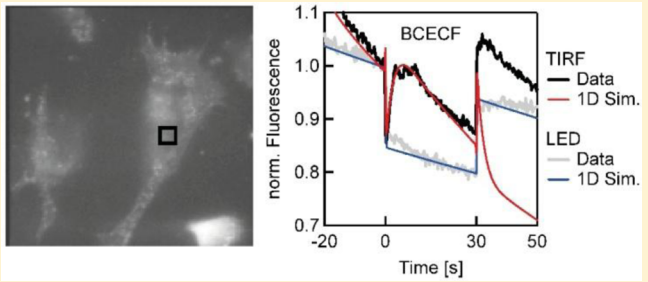

INTRODUCTION

Thermophoresis is the movement of molecules in a temperature gradient. It is sensitive even to minute binding events, allowing microscale thermophoresis (MST) to be used to measure binding affinities of DNA,[1] proteins,[2] pharmaceutical components,[3] and even membrane proteins.[4−7] When the fluorescent amino acid tryptophan is present, additional labeling of the probe can be omitted.[8] Recently, protein binding at the picomolar level was reported.[9] In contrast to enzyme-linked immunosorbent assay (ELISA), thermophoresis measurements can be conducted without surface fixation in the molecule's natural environment, such as blood serum or cell lysate.[10,11] The method was commercialized by NanoTemper Technologies (Munich, Germany) and has given many insights into complex biological systems,[12−17] including tubulin binding to transport proteins[18] and the dissociation constant of Grb2 regulating signaling.[19]

Binding affinities can be measured by thermophoresis due to its inherent dependence on a molecule's surface size, surface charge, and hydrophobic interactions. Binding of a fluorescently marked molecule, often a nucleic acid or a protein, leads to a change in the thermophoretic depletion strength. This change is measured with varying binding partner concentrations and can be directly interpreted as binding probability. A fit with the mass action law allows us to determine the binding affinity.

Besides the above *in vitro* applications, thermal gradients can transcend material boundaries and, similar to light fields, are able to probe molecules even inside living cells. For example, electrical fields are shielded by the cell membrane, so electrophoresis inside cells cannot be achieved. In order to achieve thermophoresis in living cells, the previous horizontal geometry of MST had to be adapted to cell cultures.[1,11] Here we explore a vertical gradient across a sandwich chamber. The adherent cells grow on a standard coverslip and are then inserted into the measurement setup. With this approach, *in vivo* thermophoresis from molecules inside cells can be obtained—and when thermophoresis data from inside living cells are available, binding measurements *in vivo* become a realistic goal.

A variety of other methods to measure nonbiological thermophoresis have been explored. In a plate geometry, measurements using the deflection of a laser through the chamber, heating from the top plate, conveniently suppress convection. However, they can take hours to complete, with large dimensions.[20,21] Experiments in a micrometer-sized interdigitated setup are much faster.[22] In the beam deflection method, a gradient of the refractive index is measured.[23−25] Often, this requires sample concentrations in the order of weight percent, typically hard to achieve with biological probes without aggregation artifacts. The same applies for the thermal lensing method and thermal diffusion-forced Rayleigh scattering.[26−28] In confocal microscope geometry, short distances and fast measurements are achieved.[29] The speed of axial thermophoresis was matched in order to probe strong thermal gradients.[30] With a fluorescent label, small-molecules can be measured down to picomolar concentrations.[9]

Received: June 19, 2014
Published: August 29, 2014

   dx.doi.org/10.1021/ja506169b | J. Am. Chem. Soc. 2014, 136, 15955−15960

SETUP

We used a thin sheet of solution where we applied the temperature gradient with a cold top and a warm bottom. As shown from bottom to top in Figure 1, the sample chamber consisted of a microscope slide,

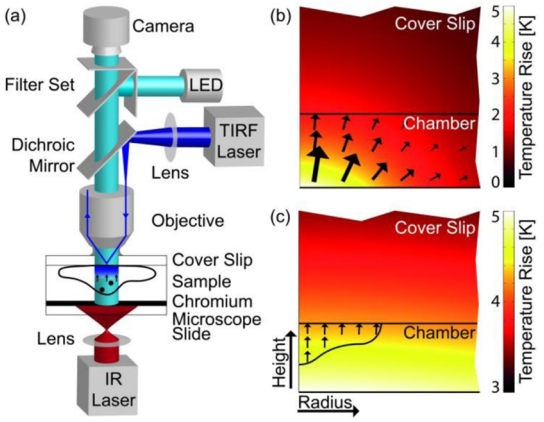

Figure 1. (a) Two illumination paths were integrated into an upright fluorescence microscope setup: normal epi-fluorescence illumination with an LED and TIRF illumination. Heating is provided from below by an IR laser that was absorbed by a chromium layer. Temperature simulations are shown here for a 10-μm-thick chamber with variable IR spot focus width: (b) 15 μm and (c) 150 μm. The thickness of the chamber in the simulations was always adapted to the experimental thickness of the chamber. The molecules move along the temperature gradient, indicated by arrows.

which was coated with chromium at the sample side to absorb the infrared laser and protective silicon oxide to prevent toxicity to the cells. The top of the sandwich structure was formed by a coverslip. A thin water film of about 20 μm prevented thermal convection. For cell measurements, the cells were grown on the coverslip in an upside-down geometry. A spot at the lower interface to the sample was heated by absorbing IR light in the chromium layer.

The fluorescence at the top of the chamber was recorded by total internal reflection fluorescence (TIRF) or epi-fluorescence illumination with a light-emitting diode (LED) through a high-numerical-aperture objective. A camera recorded the fluorescence images before, during, and after IR heating. Fluorescence detection was restricted to the top side by using TIRF microscopy, recording the upward thermophoretic movement toward the cold. In this geometry, every camera pixel can simultaneously and independently measure thermophoresis. Between measurements, the sample was left for several minutes to fully equilibrate, or it was moved to obtain measurements on an unaffected area. For further details on the setup, see the Supporting Information.

RESULTS

The temperature profile was measured using the fluorescence of the pH-sensitive dye 2′,7′-bis(2-carboxyethyl)-5-(and 6)-carboxyfluorescein (BCECF) (see Supporting Information). Under LED illumination, the lateral temperature distribution is imaged, averaging across the thickness of the chamber. The images from the camera and the known geometry were used to fit a three-dimensional finite element calculation (Figure 1b,c).

We first used polystyrene beads to confirm the thermal transport approach. In a 20-μm-high chamber with broad heating, comparably large beads with radius R = 1 μm, which are in the beginning sedimented at the bottom of the chamber, are transported during the measurement to the top side, where they are detected via fluorescence (Figure 2a). As shown for various times of the experiment, a one-dimensional finite

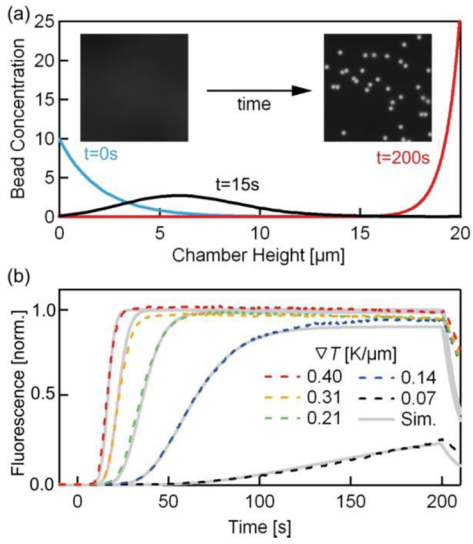

Figure 2. Imaging thermophoresis with beads. (a) Fluorescent polystyrene particles with radius R = 1 μm initially sediment and during the measurement move upward to be imaged at the top of the chamber. Simulation shown for a gradient of ∇T = 0.21 K/μm. Insets: camera images taken through the microscope, which was focused at the sample−coverslip interface. At the beginning of the thermophoresis measurement (time 0 s), the particles are sedimented to the bottom and out of focus; at the end (time 200 s), they are at the coverslip and in focus. (b) Fluorescence is used to image the concentration of the beads at the top of the chamber. With increasing thermal gradient, the transit times of the beads become shorter. All measurements are described with a thermophoretic mobility of D_T = 2.8 ± 0.5 μm^2/s·K and mass diffusion coefficient D = 0.20 μm^2/s known from the particle radius.

element simulation was used to model the combined gravitational, diffusional, and thermophoretic movement of the beads. At the top of the chamber, the thermophoresis enforces an inverted exponential sedimentation distribution.

The bead concentration at the top was detected by fluorescence. With increasing temperature gradient, the beads travel across the chamber with increasing speed, $v_T = D_T \nabla T$, while for shallow thermal gradients, they can barely overcome sedimentation, which was calculated from the weight difference to water to be $\Delta\rho$ = 60 kg/m^3 (Figure 2b). With the known mass diffusion coefficient of the beads as inferred from their radius via the Stokes−Einstein relation ($D = k_B T/6\pi\eta R$ = 0.2 μm^2/s, using the Boltzmann constant k_B, the absolute temperature T, the viscosity η, and the hydrodynamic radius R) and confirmed by literature,[31] the only fitting parameter is the thermophoretic mobility D_T, which was fitted to a constant value of 2.8 ± 0.5 μm^2(s·K) for all measured thermal gradients. The measurement setup allows probing thermophoresis for Péclet numbers larger than unity.[30] At the highest gradient of 0.2 K/μm, the Péclet number reaches $Pe = R\nabla T D_T/D$ = 2.7, indicating that the comparably large beads and the considerable thermal gradient allow for a ballistic, not a diffusional, particle movement. For the high temperature gradients, clustering at the coverslip was also observed.[30]

Before measurements were performed in cells, the thermophoresis configuration using TIRF detection was first tested with DNA, where sedimentation is not an issue (Figure 3). We study the case where focused heating (Figure 1b) combines vertical and lateral thermophoresis. With epi-fluorescence illumination using an LED, detection

dx.doi.org/10.1021/ja506169b | J. Am. Chem. Soc. 2014, 136, 15955−15960

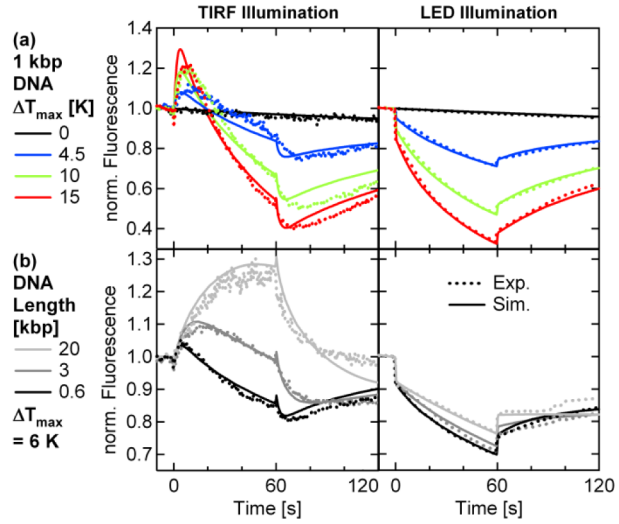

Figure 3. Focusing the IR laser to a small spot (half width at half-maximum = 65 μm) caused the molecules to move upward coaxially and outward laterally. The fluorescence above the center of the heated spot was detected with TIRF. Epi-fluorescence LED illumination did not discriminate across the chamber height. Measurements (dotted line) were conducted with (a) 1 kbp DNA in different temperature gradients and (b) different DNA lengths in the same temperature profile. Finite element simulations described the thermophoretic molecular movement in detail (solid lines).

averages across the chamber height, and only the lateral outward movement is detected. Under TIRF illumination, both the coaxial upward and lateral outward components of thermophoresis are measured.

We used DNA of different lengths as a molecular test system due to the well-established parameters. Experimental as well as simulated chamber heights were h = 13.0, 16.4, 19.3, and 25.5 μm. Measurements were performed at different thermal gradients under both TIRF and LED detection (Figure 3, dotted lines). Fluorescence at the center of the heated spot was recorded at 3 Hz. When heating is turned on (t = 0 s), fluorescence drops within <1 s due to its inherent temperature dependence. Under TIRF illumination, this drop is superimposed with the fluorescence rise due to the upward molecule movement. This fluorescence rise is later decreased by the lateral outward thermophoresis due to the focused heating spot. The thermophoretic amplitude increases for increasing temperature gradients (Figure 3a). Under epi-fluorescent LED illumination, only the temperature dependence and the lateral outward depletion of the molecules are visible. Measurements with longer DNA strands show slower diffusion, and the coaxial upward thermophoresis is detected since the lateral thermophoresis has not yet equilibrated within the heating time of 60 s (Figure 3b). After the temperature gradient is switched off (t = 60 s), back-diffusion equilibrates the thermophoretic perturbation of DNA concentration.

We quantified the DNA measurements with the known molecular parameters in a finite element simulation. The simulation model combines heat conduction, fluid flow, molecular diffusion, and thermophoresis. The geometry is modeled in cylinder coordinates; i.e., one direction is the radius, and the other is the optical axis of the experiment. Details, including all necessary physical constants, are given in the Supporting Information. Heat conduction simulates the fast temperature increase resulting from the laser illumination and predicts the thermal gradient in radial and axial directions. Since heated water shows differential density, it will show slow, laminar thermal convection that could affect the molecular profile. To rule that out, we included this effect by using the Navier–Stokes equation that models laminar fluid flow. The central part is a diffusion equation which includes the thermophoretic drift along the temperature gradients. The result is a temporal prediction of molecule concentration depending on the known timing of the heating and the unknown thermophoretic mobility D_T and the diffusion coefficient D.

The fluorescence signal recorded by the microscope is inferred from the simulated concentration, adding considerations of bleaching—different for LED or TIRF illumination—and the fast reduction of fluorescence efficiency due to the raised temperature, calibrated by measurements of fluorescence over temperature in a fluorometer. Under bright-field illumination, the concentrations are axially averaged across the chamber, while for TIRF illumination the exponential excitation volume near the coverslip is used to calculate the concentration of only the excited chromophores.

The resulting fluorescence traces fit the experimental measurements in detail over a wide range of temperature gradients and DNA lengths (Figure 3). The mass diffusion coefficient D could be determined by fitting the model to D = 14, 10, 6.0, or 2.5 $\mu m^2/s$, for the lengths of 0.6, 1, 3, and 20 kbp, respectively, which agreed with literature values.[32] The only unknown parameter was the thermophoretic mobility D_T. For the measured DNA lengths of 0.6, 1, 3, and 20 kbp, we found D_T = 2.2, 2.8, 1.5, or 1.1 $\mu m^2/s{\cdot}K$, confirming previous measurements of DNA thermophoresis.[33] The deviations of the TIRF fluorescence traces could be explained by a local deviation from the Lorenzian heating profile near the surface. It should be noted that all the traces in Figure 3a were fitted with the same parameters. Interestingly, we could fit both the coaxial and lateral thermophoresis traces with the same value for the thermophoretic mobility D_T. For details on the fits, see the Supporting Information.

We confirmed that the chromium layer absorbed all the IR light by measuring the transmission of the IR laser through the chromium-coated glass slide with a power meter (PM100USB console and S310C sensor, Thorlabs GmbH, Munich, Germany). The upward movement of the particles thus was not influenced by radiation pressure, which could add an upward force to the movement of the particles. As an additional check, we performed experiments under TIRF detection without chromium. The resulting lack of a vertical temperature gradient coincided with an undetectable vertical net movement of the molecules.

Once we fully understood the thermophoresis traces under TIRF detection and coaxial heating, we imaged thermophoresis inside living cells. The measured fluorescence traces of thermophoresis inside living HeLa cells are shown in Figure 4. On the left side, the fluorescence images from the camera are shown for representative cells. The fluorescence time traces on the right correspond to the intensities in the black squares in the cell pictures.

The IR heating laser was turned on between times 0 and 30 s. As before, the temperature dependence of the fluorophore resulted in a sudden drop of the signal after the IR laser was switched on and a sudden increase, reverting the previous drop, after heating was again switched off. As before, control measurements were conducted under epi-fluorescence LED

dx.doi.org/10.1021/ja506169b | J. Am. Chem. Soc. 2014, 136, 15955–15960

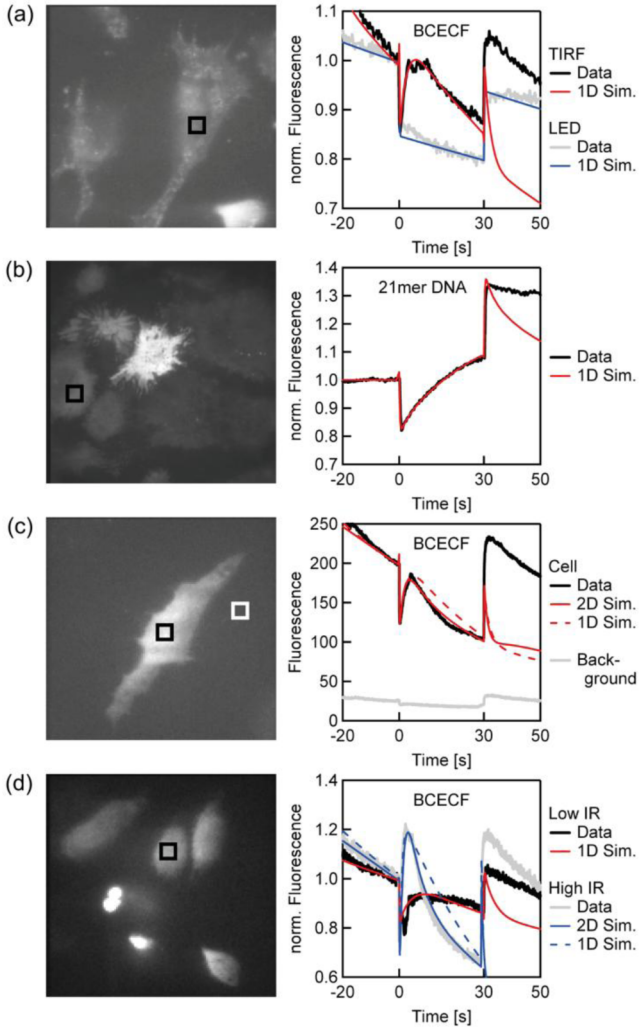

Figure 4. Thermophoresis measurements of DNA and BCECF in the cytoplasm of living cells. Thermophoresis of molecules was detected by TIRF fluorescence over time. (a) The dye molecule BCECF is moved to the cold side after a fast fluorescence decrease due to its temperature dependence. Control measurement under epi-fluorescence illumination with an LED demonstrates that the fluorescence increase stems only from the vertical movement of the fluorophore. (b) Double-stranded DNA with 21 bases showed slower thermophoresis and a larger magnitude of accumulation than BCECF. (c) The extracellular background trace is darker, does not show the thermophoresis signature, and is not affecting the thermophoresis measurement significantly. The bending of the trace is understood by the cone-shaped cell geometry. (d) Measurements in higher temperature gradients show an expected increase in the thermophoretic amplitude.

illumination. Here, an axial, upward fluorophore motion cannot be resolved and only the temperature jump is visible (Figure 4a). With LED illumination the temperature jump is slightly larger than under TIRF illumination, since the LED excites the fluorescence deeper in the chamber, where it is warmer (see Table 1). Lateral thermophoresis is also not expected due to the more defocused heating in the cell measurements (see Figure 1c). Figure 4b shows a measurement of 21-base-pair DNA, while the other measurements report the movement of the pH-sensitive dye BCECF. As before, the measurements were fitted with finite element simulations, as detailed in the Supporting Information. All parameters are listed in Table 1.

Interestingly, the diffusion of BCECF was found to be $D = 3\ \mu m^2/s$, considerably slower than the free buffer values from the cytoplasm of 100 $\mu m^2/s$ reported using FRAP analysis of the mobile fraction.[34] For the measurements with 21mer double-stranded DNA, we find a diffusion coefficient of 0.1 $\mu m^2/s$, also lower than the reported 20 $\mu m^2/s$.[35] Since this method actively moves the molecules, it measures the average over all fractions, mobile and possibly immobile. The main contribution to slowing down diffusion is thought to be the collisions with other macromolecules.[35,36] Therefore, a size-dependent further reduction of these values is expected when thermophoresis of biomolecules bound to other molecules is considered. We also tried to measure larger molecules (ribosomes with green fluorescent protein label), but the reduction of diffusion made it impossible to detect sufficient thermophoretic movement. Diffusion through the cytoplasm is a prerequisite for thermophoresis. The ribosome is so large, and bound to the endoplasmic reticulum, that its movement is hindered. In a 5 μm high cell, the smallest effective diffusion coefficient which should be measurable within 5 min is about $D = (5\ \mu m)^2/5\ min = 0.08\ \mu m^2/s$. Thermophoresis, in contrast to all other techniques, actively moves the molecules and therefore probes their mobility on a global scale. As a result, interactions with the cytoplasm at a larger scale can be probed by thermophoresis.

Interestingly, for BCECF, the thermophoretic mobility is only slightly affected by the cell. The measured value of $D_T = 4.4 \pm 2\ \mu m^2/(s \cdot K)$ is compatible with the reported *in vitro* value of $D_T = 7.5\ \mu m^2/(s \cdot K)$.[27] In contrast, the DNA probe is reduced in both diffusion and thermophoretic mobility, with a value of $D_T = 0.12\ \mu m^2/(s \cdot K)$ as compared to the literature value of $D_T = 1\ \mu m^2/(s \cdot K)$.[37] These measurements suggest that molecular interactions inside a cell can be differentiated between affecting thermophoretic mobility or diffusivity. Recent models of thermophoresis predict values for the Soret coefficient $S_T = D_T/D$ based on the energetics of temperature-dependent electrical fields in the vicinity of the molecules.[37,38] One can expect that molecular crowding inside a cell will affect these electrical fields in a very similar way. Indeed, while the diffusion coefficient D of BCECF and DNA is differentially affected by the intracellular situation, possibly due to different interactions with cellular components and different effects due to the different molecular sizes, the Soret coefficient for both molecules is increased similarly by a factor of about 20 from the *in vitro* situation. So the differential changes of D_T for BCECF and DNA seem to merely compensate the different diffusion coefficients. This indicates that also within cells, S_T seems to be the dominant parameter to describe thermophoresis, not D_T, while D is simply given by steric interactions.

In Figure 4c,d, the thermophoresis traces show a curved fluorescence decrease during thermophoresis which could not be readily explained, even with TIRF bleaching dynamics in the 1D simulations (broken line). We propose that this effect is due to the inhomogeneous thickness of the individual cell, leading to a temporary buildup of lateral concentration inhomogeneities within the cells that subsequently equilibrate. We modeled such a cell in a 2D radial geometry, as a cone with height 10 μm and radius 20 μm, the readout being above the center, but still with a purely vertical, constant temperature gradient. This 2D model could explain the curved cell traces (see Supporting Information).

dx.doi.org/10.1021/ja506169b | J. Am. Chem. Soc. 2014, 136, 15955−15960

Table 1. Parameters Used for the Simulations in Figure 4[a]

Figure 4 panel	molecule	∇T [K/μm]	$\Delta T\ \alpha$ [%]	h [μm]	v_T [μm/s]	D_T [$\mu m^2/(s\cdot K)$]	k_{bleach} [%/s]	D [$\mu m^2/s$]
(a) TIRF	BCECF	0.076	***20***	8	***0.24***	3.2	***15***	***3***
(a) LED	BCECF	0.076	***15***	8	***0.24***	3.2	***0.2***	***3***
(c) 1D	BCECF	0.17	***45***	8	***0.60***	3.6	***35***	***3***
(c) 2D	BCECF	0.17	***45***	cone	***0.66***	4.0	***15***	***3***
(d) 1D	BCECF	0.034	***21***	10	***0.15***	4.4	***13***	***3***
(d) 2D, 5×IR	BCECF	0.17	***47***	cone	***1.32***	8.0	***10***	***4***
(b) 1D	DNA	0.17	***22***	5	***0.02***	0.12	***0***	***0.1***

[a]At various laser power, different temperature gradients ∇T were applied. The temperature dependence α of the fluorophore used was fitted but not calibrated due to an unknown pH dependence upon temperature changes inside the cell. The thermophoretic mobility of BCECF and DNA could be determined from the thermophoretic velocity v_T used to fit the fluorescence transients. We implemented bleaching for TIRF and LED illumination in the simulation with a bleaching rate k_{bleach}. TIRF illumination only bleached the fluorophores close to the coverslip, with a penetration depth of λ = 200 nm. The chamber height is denoted with h. Columns shown in boldface italic denote fitting parameters; others are measured or derived values.

Background fluorescence could be measured next to a cell (Figure 4c, white box). Even for this example of high background levels compared to the non-cell measurements, its minor dynamics upon heating did not significantly affect the thermophoretic analysis.

The setup geometry is capable of simultaneously measuring vertical thermophoresis in cells at various positions in the field of view of the camera. For the molecular systems used, we neither expected nor recorded significant deviations of D_T and D across the image of the cell. It is interesting to note that the re-allocation of the molecules by thermophoresis resulted in a greatly reduced kinetics of the back-diffusion dynamics, which could not be fully accounted for by the thermophoretic model for the cell measurements, whereas they were perfectly understood for the measurements without the cells. This points to a not yet understood cellular dynamics induced by the global application of a temperature field. One should note that the cells are located at the cold side of the chamber.

In Figure 4d, traces with different heating intensities are shown. At a 5-fold higher temperature gradient, larger thermophoretic amplitude is found after the also-increased temperature jump. The diffusion coefficient is not affected, and traces are well fitted by the thermophoretic model. Thermophoretic mobility increases slightly more than expected from temperature-dependent *in vitro* data,[33,37] indicating that binding inside the cell is decreased by the increased temperature.

Depending on the cell height, different chamber designs are appropriate. For example, measurements in adherent bacteria seem possible but would require steep thermal gradients. For this, a more efficient heat sink would be advantageous, possibly provided by sapphire coverslips. Also, a more focused heating would reduce the overall sample heating.

We have shown here that thermophoresis in cells can be recorded two-dimensionally. As discussed, the cell shape can affect the thermophoresis signal. To perform binding assays, one has to use cells with a homogeneous cell shape. Another option is to revert to a dual-color, competitive assay where a mutant nonbinding species is compared against a binding species, both labeled, for example, with GFP and YFP. This technique would be especially suited for the measurement of pharmaceutical compounds that bind to intracellular targets. These compounds permeate the cell membrane, and therefore the binding titration could be performed on a high-throughput basis. Another option to consider is to combine IR heating with TIRF illumination and perform heating and imaging from one side. This would also allow measurements in an open format, such as multi-well plates.

CONCLUSION

In this work, thermophoresis was performed inside living cells for the first time. We have developed a TIRF-based measurement geometry which allows us to perform thermophoresis measurements with two-dimensional resolution on the micrometer scale. We compare our results with known epifluorescence measurements of the thermophoresis of DNA and show that the physical processes involved in this geometry can be quantitatively understood. Furthermore, we present data from thermophoresis measurements of fluorescent dyes and DNA inside living cells acquired with the vertical thermophoresis setting. Biomolecular binding studies are already conducted in cell lysate.[11] Comparable to electrophoresis in vitro, thermophoresis has the potential to perform in vivo measurements of various fluorescently labeled biomolecules inside of living cells. Since the method shown here allows for parallel imaging with micrometer resolution and is able to resolve thermophoretic mobilities and diffusion coefficients, further developments bode well for allowing the quantification of biomolecule affinities inside living cells.

ASSOCIATED CONTENT

Supporting Information

Details of setup, chamber, optics, bead measurements, temperature profiles, DNA measurements, cell culture, cell transfection, and measurements; finite element calculations of temperature field model, bead thermophoresis model, DNA thermophoresis model, and intracellular thermophoresis model. This material is available free of charge via the Internet at http://pubs.acs.org.

AUTHOR INFORMATION

Corresponding Author

dieter.braun@lmu.de

Notes

The authors declare no competing financial interest.

ACKNOWLEDGMENTS

We thank Hermann Gaub and Angelika Kardinal for the cell culture. Funding from SFB 1032 Project A4 and the Nanosystems Initiative Munich is gratefully acknowledged.

REFERENCES

(1) Baaske, P.; Wienken, C. J.; Reineck, P.; Duhr, S.; Braun, D. *Angew. Chem., Int. Ed.* **2010**, *49*, 2238.
(2) Wienken, C. J.; Baaske, P.; Rothbauer, U.; Braun, D.; Duhr, S. *Nat. Commun.* **2010**, *1*, 100.
(3) Pollack, S. J.; Beyer, K. S.; Lock, C.; Müller, I.; Sheppard, D.; Lipkin, M.; Hardick, D.; Blurton, P.; Leonard, P. M.; Hubbard, P. A.; Todd, D.; Richardson, C. M.; Ahrens, T.; Baader, M.; Hafenbradl, D. O.; Hilyard, K.; Bürli, R. W. *J. Comput. Aided Mol. Des.* **2011**, *25*, 677.
(4) Corin, K.; Baaske, P.; Ravel, D. B.; Song, J.; Brown, E.; Wang, X.; Geissler, S.; Wienken, C. J.; Jerabek-Willemsen, M.; Duhr, S.; Braun, D.; Zhang, S. *PLoS One* **2011**, *6*, e23036.
(5) Xiong, X.; Coombs, P. J.; Martin, S. R.; Liu, J.; Xiao, H.; McCauley, J. W.; Locher, K.; Walker, P. A.; Collins, P. J.; Kawaoka, Y.; Skehel, J. J.; Gamblin, S. J. *Nature* **2013**, *497*, 392.
(6) Parker, J. L.; Newstead, S. *Nature* **2014**, *507*, 68.
(7) Srinivasan, V.; Pierik, A. J.; Lill, R. *Science* **2014**, *343*, 1137.
(8) Seidel, S. A. I.; Wienken, C. J.; Geissler, S.; Jerabek-Willemsen, M.; Duhr, S.; Reiter, A.; Trauner, D.; Braun, D.; Baaske, P. *Angew. Chem., Int. Ed.* **2012**, *51*, 10656.
(9) Jerabek-Willemsen, M.; André, T.; Wanner, R.; Roth, H. M.; Duhr, S.; Baaske, P.; Breitsprecher, D. *J. Mol. Struct.* **2014**, DOI: 10.1016/j.molstruc.2014.03.009.
(10) Lippok, S.; Seidel, S. A. I.; Duhr, S.; Uhland, K.; Holthoff, H.-P.; Jenne, D.; Braun, D. *Anal. Chem.* **2012**, *84*, 3523.
(11) Seidel, S. A. I.; Dijkman, P. M.; Lea, W. A.; van den Bogaart, G.; Jerabek-Willemsen, M.; Lazic, A.; Joseph, J. S.; Srinivasan, P.; Baaske, P.; Simeonov, A.; Katritch, I.; Melo, F. A.; Ladbury, J. E.; Schreiber, G.; Watts, A.; Braun, D.; Duhr, S. *Methods* **2013**, *59*, 301.
(12) Shang, X.; Marchioni, F.; Evelyn, C. R.; Sipes, N.; Zhou, X.; Seibel, W.; Wortman, M.; Zheng, Y. *Proc. Natl. Acad. Sci. U.S.A.* **2013**, *110*, 3155.
(13) Alexander, C. G.; Jurgens, M. C.; Shepherd, D. A.; Freund, S. M. V.; Ashcroft, A. E.; Ferguson, N. *Proc. Natl. Acad. Sci. U.S.A.* **2013**, *110*, E2782.
(14) Chen, Z.; Vohidov, F.; Coughlin, J. M.; Stagg, L. J.; Arold, S. T.; Ladbury, J. E.; Ball, Z. T. *J. Am. Chem. Soc.* **2012**, *134*, 10138.
(15) Patnaik, S.; Zheng, W.; Choi, J. H.; Motabar, O.; Southall, N.; Westbroek, W.; Lea, W. A.; Velayati, A.; Goldin, E.; Sidransky, E.; Leister, W.; Marugan, J. J. *J. Med. Chem.* **2012**, *55*, 5734.
(16) Shoji, T.; Saitoh, J.; Kitamura, N.; Nagasawa, F.; Murakoshi, K.; Yamauchi, H.; Ito, S.; Miyasaka, H.; Ishihara, H.; Tsuboi, Y. *J. Am. Chem. Soc.* **2013**, *135*, 6643.
(17) Wang, T.; Bisson, W. H.; Mäser, P.; Scapozza, L.; Picard, D. *J. Med. Chem.* **2014**, *57*, 2524.
(18) Bhogaraju, S.; Cajanek, L.; Fort, C.; Blisnick, T.; Weber, K.; Taschner, M.; Mizuno, N.; Lamla, S.; Bastin, P.; Nigg, E. A.; Lorentzen, E. *Science* **2013**, *341*, 1009.
(19) Lin, C.-C.; Melo, F. A.; Ghosh, R.; Suen, K. M.; Stagg, L. J.; Kirkpatrick, J.; Arold, S. T.; Ahmed, Z.; Ladbury, J. E. *Cell* **2012**, *149*, 1514.
(20) Snowdon, P. N.; Turner, J. C. R. *Trans. Faraday Soc.* **1960**, *56*, 1409.
(21) Chan, J.; Popov, J. J.; Kolisnek-Kehl, S.; Leaist, D. G. *J. Solution Chem.* **2003**, *32*, 197.
(22) Putnam, S. A.; Cahill, D. G.; Wong, G. C. L. *Langmuir* **2007**, *23*, 9221.
(23) Piazza, R.; Guarino, A. *Phys. Rev. Lett.* **2002**, *88*, 208302.
(24) Braibanti, M.; Vigolo, D.; Piazza, R. *Phys. Rev. Lett.* **2008**, *100*, 108303.
(25) Vigolo, D.; Buzzaccaro, S.; Piazza, R. *Langmuir* **2010**, *26*, 7792.
(26) Iacopini, S.; Rusconi, R.; Piazza, R. *Eur. Phys. J. E* **2006**, *19*, 59.
(27) Köhler, W. *J. Chem. Phys.* **1993**, *98*, 660.
(28) Kishikawa, Y.; Shinohara, H.; Maeda, K.; Nakamura, Y.; Wiegand, S.; Kita, R. *Phys. Chem. Chem. Phys.* **2012**, *14*, 10147.
(29) Jung, H.; Gusev, V. E.; Baek, H.; Wang, Y.; Diebold, G. J. *Phys. Lett. A* **2011**, *375*, 1917.
(30) Weinert, F. M.; Braun, D. *Phys. Rev. Lett.* **2008**, *101*, 168301.
(31) Wiseman, P. W.; Squier, J. A.; Ellisman, M. H.; Wilson, K. R. *J. Microsc.* **2000**, *200*, 14.
(32) Pluen, A.; Netti, P. A.; Jain, R. K.; Berk, D. A. *Biophys. J.* **1999**, *77*, 542.
(33) Duhr, S.; Braun, D. *Proc. Natl. Acad. Sci. U.S.A.* **2006**, *103*, 19678.
(34) Kao, H. P.; Abney, J. R.; Verkman, A. S. *J. Cell Biol.* **1993**, *120*, 175.
(35) Dauty, E.; Verkman, A. S. *J. Biol. Chem.* **2005**, *280*, 7823.
(36) Lukacs, G. L.; Haggie, P.; Seksek, O.; Lerchardeur, D.; Freedman, N.; Verkman, A. S. *J. Biol. Chem.* **2000**, *275*, 1625.
(37) Reichl, M. R.; Herzog, M.; Götz, A.; Braun, D. *Phys. Rev. Lett.* **2014**, *112*, 198101.
(38) Mast, C. B.; Schink, S.; Gerland, U.; Braun, D. *Proc. Natl. Acad. Sci. U.S.A.* **2013**, *110*, 8030.